02

Fluorescent diamond microcrystals with NV^- centers for applications in photonics and sensors: identification and photophysical signatures

© V.Yu. Osipov[1], F.M. Shakhov[1], K.V. Bogdanov[2], K. Takai[3], A.V. Baranov[2]

[1] Ioffe Institute,
194021 St. Petersburg, Russia
[2] ITMO University,
197101 St. Petersburg, Russia
[3] Department of Chemical Science and Technology, Hosei University,
Koganei, 184-8584 Tokyo, Japan

e-mail: osipov@mail.ioffe

Received November 21, 2023
Revised November 21, 2023
Accepted November 30, 2023

Synthetic microcrystalline Ib HPHT diamonds synthesized using a nickel-containing catalyst and containing fluorescent negatively charged nitrogen-vacancy (NV^-) centers, specially introduced by irradiation with high-energy electrons, were studied. A set of identification signatures corresponding to diamond microcrystals with high optical brightness and a concentration of NV^- centers of about 4.5 ppm is shown. Electron paramagnetic resonance signals for nitrogen impurity atoms in the neutral state and nickel in the -1 charge state depend on temperature according to Curie's law, while the signal $g = 4.295$ (W15), associated with $\Delta m_s = 2$ transitions in the NV^- center, demonstrates a different type temperature behavior. Illumination of microcrystals with light in the spectral range of $1.38-2.95$ eV at $T = 100$ K entails optical spin polarization for the $m_s = 0$ level of the ground unexcited state of $^3A_2$ NV^- centers. Synthesized diamond microcrystals can be used in photonics devices.

Keywords: Diamond microcrystals, nitrogen-vacancy centers, paramagnetic centers, luminescence, electron paramagnetic resonance.

DOI: 10.61011/EOS.2023.12.58177.5776-23

Introduction

Synthetic diamond is an excellent matrix for creating optical centers characterized by luminescence with a high quantum yield, luminescence stability, and no degradation over a long time [1,2]. For synthetic Ib HPHT diamonds produced at high pressure and temperature using a nickel-containing catalyst, the main optical centers are usually complexes based on impurity nitrogen, carbon vacancies, and impurity nickel in substitutional positions in the diamond lattice [3–6]. Among them, the main optical center, actively studied over the past 20 years, is a nitrogen-vacancy pair NV^- in a negatively charged state [7]. To obtain such centers in a diamond matrix in the amount of $4-10$ ppm sufficient for practical applications, microcrystals are usually irradiated with a beam of high-energy ($> 2-3$ MeV) electrons and annealed at a temperature of about 900°C [8,9]. At this temperature, vacancies created in the diamond matrix become mobile and, during the annealing process, are captured by impurity nitrogen atoms fixed in the lattice. Substitutional impurity nitrogen atoms, present in the lattice in excess quantities (up to 200 ppm), are electron donors; as a result, NV^- centers acquire a negative charge. On the basis of this center, over the past 15 years, various sensors of physical fields and influences, such as magnetic field, temperature, pressure, etc., have been proposed, as well as optical circuits have been developed that exploit the properties of entangled states of photons emitted by individual NV^- centers for quantum cryptography applications [10–17]. In addition, diamond nanoparticles up to 50 nm in size carrying NV^- centers in sufficient concentrations can be used for fluorescence imaging of cell organelles and submicron inclusions in cells [18]. Red radiation of NV^- centers falls into the transparency window of biological tissues and comes out well from their thin layers. The use of Ib HPHT diamonds with NV^- centers as sensors of physical fields and quantities implies their integration into optical circuits for excitation and output of fluorescent radiation and positioning of a matrix with centers in the diagnostic zone of the corresponding physical field. These conditions can be easily implemented, for example, by placing single crystallites with NV^- centers at the end of optical fiber or inside the central core of optical fiber that channels optical radiation directly [19]. In this regard, it is important to study the parameters of diamond crystals with NV^- centers in the size range from $1-2$ to 30 μm.

Modern industry, which uses the method of high pressures and high temperatures to synthesize diamonds, mainly produces microcrystalline diamonds for mechanical applications (cutting, drilling, grinding, etc.), and such materials are subject only to requirements as to hardness, thermal conductivity, and, in some cases, the microcrystal habitus. However, synthetic diamonds for applications in

photonics and sensors should be manufactured according to special requirements with a targeted improvement of their properties, including high quality of the crystal lattice; lack of dislocations, foreign inclusions, and mechanical stresses; and, in particular, such a distribution of active impurities in the matrix that yields no cluster forms of these impurities (most importantly, cluster forms of nitrogen and nickel nanoparticles). It bears reminding that nickel enters a growing crystal from the melt of the catalyst metal used in diamond synthesis, and nitrogen enters the crystal lattice uncontrollably from air in the synthesis chamber and in the finely dispersed graphite precursor powder. To controllably reduce the concentration of nitrogen impurities in the diamond matrix, metal nitrogen getters (for example, aluminum added to the graphite charge) are commonly used. Nitrogen and nickel impurities are well identified in the diamond lattice by electron paramagnetic resonance (EPR). Specifically, EPR signals of nitrogen in diamond were discovered by Smith and co-workers in 1959 [20], and signals from nickel in carbon substitutional positions in the diamond lattice were discovered by Loubser and van Ryneveld in 1966 [21]. The centers responsible for this signal were identified as the $3d^7$ electronic configuration of a Ni^- ion (with spin $S = 3/2$) by Isoya and co-workers only in 1990 [22]. Despite the fact that isolated centers associated with nitrogen and nickel in diamond have been known for many decades, certain specifics of their characteristics in Ib HPHT microcrystals designed specially for photonics applications are still insufficiently studied and characterized by existing combined techniques.

In the present paper, we report certain characteristics of high-quality Ib HPHT diamonds with NV^- centers that have excellent emission properties and can be considered as a reference. The characteristics discussed below can be considered necessary for the selection of high-quality synthetic diamond microcrystals with NV^- centers for applications in sensor and telecommunication devices. The work examines the EPR signals for NV^- centers, paramagnetic nitrogen (N_S^0), and nickel impurities in charge state 1- as a function of temperature and photoexcitation with broadband light from a halogen lamp.

Samples and experimental methods

Synthetic Ib HPHT diamond microcrystals grown and processed by Columbus Nanoworks Ltd. (USA) were studied. Crystals as large as $350\,\mu$m were synthesized at high pressures (5–6 GPa) and temperatures (1300–1600°C) by the temperature gradient method using microcrystalline graphite as a carbon precursor, nickel-containing catalyst, and diamond seeds (nucleation centers). In this process, graphite dissolves in the molten catalyst, and carbon atoms migrate to the colder zone of the melt, create a supersaturated solution-melt in this area, and crystallize on diamond seeds, forming diamond crystals up to several hundred micrometers in size. The non-diamond phase is removed after synthesis by treating the material in boiling acids. NV^- centers were created by irradiating the synthesized material with a beam of high-energy (> 2 MeV) electrons (absorbed dose of at least $7 \cdot 10^{18}\,e^-/cm^2$) followed by annealing at a temperature of 800°C for several hours. During irradiation, the electron beam current was 25 mA, and the area of the cooled surface with irradiated diamond powder was $\sim 770\,cm^2$. To remove parasitic ferromagnetic impurities entering the material during irradiation and annealing, secondary treatment in boiling acids was performed. The non-irradiated material was uniquely named #7381-un, and the irradiated and annealed material was named #7381-irr/ann. Irradiated and annealed microcrystals with NV^- centers were additionally milled to an average size of $\sim 13-14\,\mu$m and purified in acids from metallic inclusions that entered the material in the process of milling with metal balls. To remove sp^2- fragments formed on the surface of particles as a result of its construction during intensive milling, powders were subjected to oxidation in air at a temperature of 450°C. The particle size spread in the powder was $\sim 4-35\,\mu$m. Certain details of the procedures for irradiation and milling of diamond microcrystals can also be found in [23–25]. The approximate concentration of NV^- centers in irradiated and annealed microcrystals was at least 4 ppm (based on an estimate of the absorbed dose from electron irradiation), and the concentration of substitutional nitrogen impurities in non-irradiated crystals was 140 ± 10 ppm (based on the manufacturer's data). Processed crushed microcrystals were a powder of light purple (or white) color. The sample obtained using electron irradiation, annealing, and milling was given the unique name #7381-*bis*. The optical image of milled #7381-*bis* fluorescent microcrystals is shown in Fig. 1. It was obtained with a Nikon Eclipse Ti-S epifluorescence inverted microscope using a „Texas Red Filter Cube" combined optical filter with an emission bandwidth of 600–660 nm, an excitation bandwidth of 542–582 nm, and a 593 nm dichroic cutoff filter.

The effect of milling on the phonon modes and the impurity background of crushed Ib HPHT diamond microcrystals was studied by analyzing the infrared (IR) absorption spectra of two different fractions of diamond powders with average particle sizes $8 \pm 2\,\mu$m and $70 \pm 10\,\mu$m obtained from the same precursor material (diamond microcrystals $200-350\,\mu$m in size). Purified fractions of MSY 6–10 micron (lot 20048, ref. 7771) and MSY 60–80 micron (lot P19102, ref. 7772) monocrystalline diamond powders were supplied by Microdiamant AG (Lengwil, Switzerland).

Infrared absorption spectra of powder samples were recorded using an Infralum FT-08 spectrometer (Russia) fitted with a Pike EASIDIFF ™ attachment in the diffuse reflection mode (DRIFT) with a resolution of 4 cm^{-1} and a number of scans of 100. The baseline was determined by selecting an analytical function such that the line „of zero" absorption passed through the absorption minima in the spectra near the points of ~775, ~1530, and ~2680 cm^{-1} and one point chosen at the high-frequency (at $\sim 4000\,cm^{-1}$) or

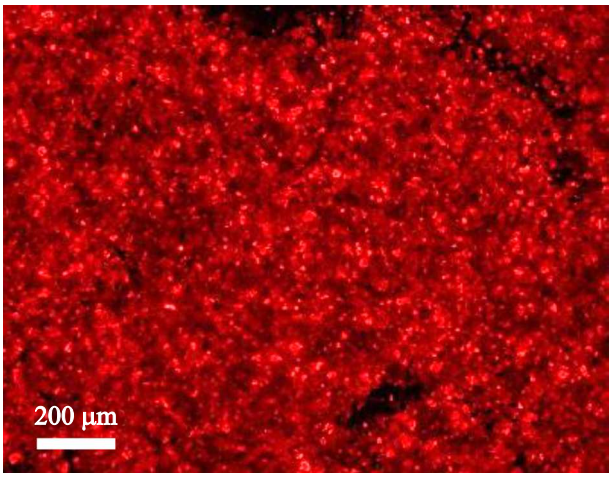

Figure 1. Optical image of milled fluorescent diamond microcrystals obtained by exciting irradiation in the spectral band of 542−582 nm and recording in the 600−660 nm band.

low-frequency (at 615 cm^{-1}) edge of the spectral interval. The nitrogen content was estimated from the amplitude of the narrow absorption peak at $\sim$ 1344 cm^{-1} corresponding to local vibrational modes of C–N bonds in the diamond lattice. The powder material to be examined was loaded into cuvettes with an inner diameter of 10 mm and a depth of 2.3 mm.

EPR spectra were recorded using an X-band JEOL-JES-FA300 EPR spectrometer (Japan) fitted with a flow-type cryostat from Oxford Instruments (UK). The microwave frequency was $\sim$ 9.04 GHz. Samples were poured into quartz tubes with an outer diameter of 4 mm and sealed at the upper end against the possible influx of water vapor and paramagnetic oxygen at low temperatures. Liquid nitrogen vapor was used to cool the sample in the resonator. Temperature stabilization in the range of 100−210 K was carried out with an accuracy of 0.03 K. The EPR spectra were recorded without and with illumination. The spectra were recorded with the following parameters: magnetic field modulation, 0.03 or 0.07 mT; modulation frequency, 100 kHz; time constant, 30 ms; and microwave power, 0.001 or 0.010 mW. The sample was illuminated with a 500 W xenon lamp (Ushio Lighting Inc.) through an HA30 optical filter with a bandwidth of 300−900 nm produced by Hoya Candeo Optronics Corporation (Saitama, Japan). The spectral composition of radiation was changed, if necessary, by Hoya L42 and R64 cutoff optical filters with cutoff wavelengths of about 420 and 640 nm. The magnetic field was measured using a built-in Hall sensor placed on one of the poles of the electromagnet. The g-factors of the corresponding resonance lines were calculated with additional correction of the magnetic field sweep intervals and, consequently, the magnitude of the resonance magnetic field (within $-0.10\ldots+0.36$mT) using an NMR magnetic field sensor.

Luminescence spectra were recorded with an „inVia“ micro-Raman setup (Renishaw, UK) using exciting laser radiation with a wavelength of 488 nm and a 50$^{\times}$ microlens. Exciting radiation was focused into a spot with a diameter of $\sim 2\,\mu$m on the surface or at some depth below the surface of a single microcrystal. Luminescent radiation was collected in backscattering geometry from the sample surface. The spectrum from each individual microcrystal was recorded in five accumulations. The exposure time of a single accumulation was 10 s. When studying the luminescence of particles with intentionally created NV^- centers, the intensity of excitation radiation was chosen to be 0.0001% of the maximum achievable in the setup used ($\sim$ 5−8 mW). Characteristic luminescence spectra for individual particles were plotted for the most representative data collected from a set of 7−10 microcrystals of the same type and size.

Results and discussion

Infrared spectroscopy of crushed diamonds

To test the effect of milling on the crystalline quality of produced diamond particles, the IR absorption spectra of two fractions of diamond powders with average particle sizes of 8 and 70 μm were studied. These spectra are presented in Fig. 2, *a* in the spectral range of 700−2800 cm^{-1} by curves *1* and *2*. The range of 2800−4000 cm^{-1} is complicated by the presence of extended absorption bands from adsorbed water and is therefore not presented for analysis. For the large-size fraction of diamond particles, Fig. 2, *b* additionally shows an absorption line at 1344 cm^{-1} in high resolution. The width of this line at half maximum is $\sim$ 4.7 cm^{-1}.

The spectra of coarse and fine size fractions are similar to each other and differ only in minor details. The spectra of both particle fractions (spectra *1* and *2*) show characteristic broad bands of a specific shape (1700−2700 cm^{-1} range) corresponding to the fundamental two-phonon lattice absorption of diamond, broad structured bands of impurity absorption (700−1500 cm^{-1} range), and narrow lines (at 1344 cm^{-1}) corresponding to absorption on local vibrations of C–N bonds and caused by the presence of isolated substitutional nitrogen impurities in the covalent lattice of diamond. The modes of local vibrations are mainly due to vibrations of carbon atoms adjacent to a nitrogen atom in the lattice [26]. The narrow line at 1344 cm^{-1} in the spectrum is a specific marker of the presence of substitutional nitrogen atoms in the material, and its intensity (relative to the intensity of the fundamental two-phonon absorption band) or ratio A_{1344}/A_{1994} of intensities of the absorption bands can be used to estimate the concentration of substitutional nitrogen in the diamond crystal. Here, 1994 cm^{-1} is the wave number corresponding to the local minimum between the neighboring peaks (1977 and 2030 cm^{-1}) of the low-frequency lattice absorption band. The 1130 cm^{-1} band is also due to the presence of isolated substitutional nitrogen

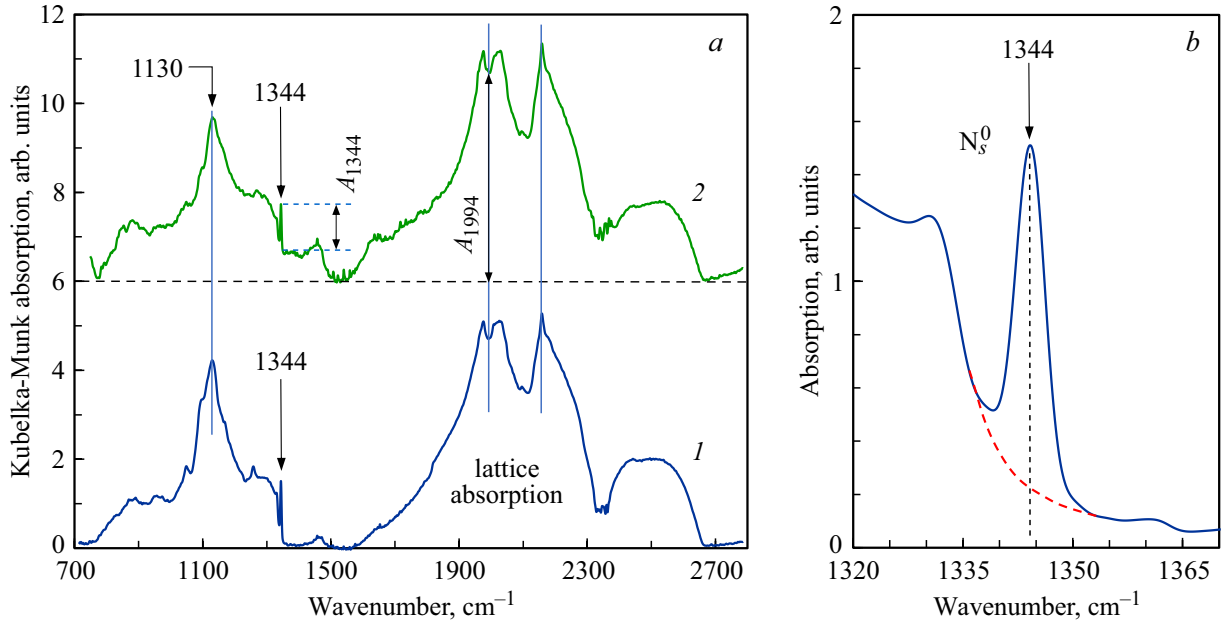

Figure 2. IR absorption spectra (a) of two fractions of Ib HPHT diamond microcrystals with average sizes of 70 (1) and 8 μm (2) and a narrow $\sim 1344\,\text{cm}^{-1}$ absorption line (b) corresponding to local C–N bond vibrations in microcrystals of the $70 \pm 10\,\mu$m size fraction. Panel (a): spectrum 2 is shifted vertically by 6 units.

impurities in the lattice, and its intensity can also be used to estimate the nitrogen concentration [27,28]. The following empirical relationship between the concentration of isolated nitrogen atoms $[N_S^0]$ (in ppm) and optical absorption coefficient μ_{1344} expressed in cm^{-1} holds true for bulk diamond: $[N_S^0] = 37.5\mu_{1344}$ [29,30]. At room temperature, the lattice absorption for light with a wavenumber of $1994-2000\,\text{cm}^{-1}$ is about $10\,\text{cm}^{-1}$ [31–33] [1]. Therefore, the absolute absorption at local vibrations of C–N bonds (at 1344 cm^{-1}) can be calculated using the formula $\mu_{1344} = (A_{1344}/A_{1994}) \cdot 10\,\text{cm}^{-1}$. Here, absorption intensities A_{1344} and A_{1994} expressed in relative units are determined directly from the absorption spectra, as shown in Fig. 2. Recording an IR spectrum together with the lattice absorption band, one can determine the absolute absorption of the material in the impurity band without measuring absolute absorption coefficients. Various modifications of the $[N_S^0]$ estimation method along with the corresponding formulae are described in [30,32,34]. For microcrystals ~ 70 and $\sim 8\,\mu$m in size, the corresponding nitrogen concentration is about $\sim 95 \pm 10$ ppm. It is interesting to note that for the powder with smaller diamond particles $\sim 0.5-1\,\mu$m in size obtained by milling from the same starting material as the large-sized fractions, the two-phonon lattice absorption band is much weaker compared to prevalent absorption by surface functional groups in the $900-1650\,\text{cm}^{-1}$ range. The absorption line from substitutional nitrogen (at $1344\,\text{cm}^{-1}$) is lacking (or not observed) in the spectrum of such particles. Thus, this method for determining the concentration of nitrogen impurities in the material works well for diamond powders with an average particle size of $8\,\mu$m and above, but is not applicable to diamond powders with an average particle size below $1\,\mu$m. It is clear that a reduction in the size of diamond crystallites does not significantly change the spectrum of phonon states in crystals (unless the particle size drops below a few micrometers).

[1] According to [32,33], the absorption at $\sim 2000\,\text{cm}^{-1}$ is about $12.5\,\text{cm}^{-1}$.

Luminescence of irradiated and non-irradiated samples

Figure 3 shows the normalized luminescence spectra of two microcrystals #7381-un and #7381-irr/ann obtained at excitation radiation intensities of 0.5 and 0.0001% of the maximum achievable at the crystallite surface in the setup used. Normalization was carried out by the luminescence intensity at a wavelength of 710 nm.

A detailed examination shows that both samples have NV^- centers and their luminescence spectra are almost identical, but the luminescence intensity of irradiated and annealed sample #7381-irr/ann is about 450–500 times higher under the same excitation conditions than the luminescence intensity of non-irradiated sample #7381-un, where NV^- centers are formed in the process of HPHT synthesis in very small amounts (e.g., at the level of 10 ppb or less). The luminescence intensity of the #7381-un sample at the maximum of the 640–800 nm spectral band is comparable (with accuracy to a factor of 3) to the intensity of the Raman scattering line at $\lambda = 521.93$ nm [2]. If we assume that the #7381-un sample contains NV^-

[2] The 521.93 nm line corresponds to a Raman shift of $1332.14\,\text{cm}^{-1}$.

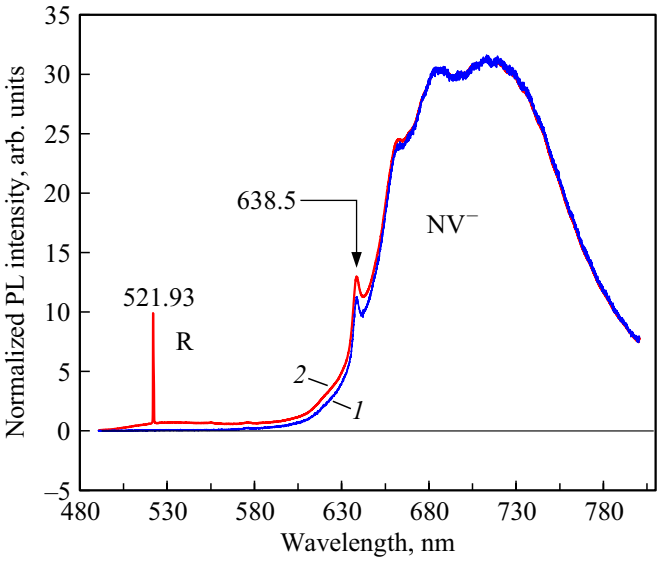

Figure 3. Normalized photoluminescence spectra of two individual microcrystals selected from #7381-irr/ann (*1*) and #7381-un (*2*) powders. The wavelength of the excitation laser is $\lambda_{ex} = 488$ nm. R is the Raman line of diamond ($\lambda = 521.93$ nm). Zero-phonon luminescence lines of NV^- centers at 638.5 nm and identical side phonon bands (650–800 nm) are seen clearly in both spectra. Temperature $T = 293$ K.

centers in an amount of 8–10 ppb[3], then sample #7381-irr/ann contains them in an amount of 4–5 ppm. It is well known that the main share of emission from NV^- centers at room temperature falls within the spectral interval of 650–850 nm (i.e., the side phonon band) and the narrow zero phonon line at 638 nm accounts for less than 10% of the total emission intensity. Since the emission spectra of NV^- centers for irradiated and non-irradiated samples are practically identical in the spectral band above 650 nm, it can be concluded that the absorbed dose of irradiation by high-energy electrons has almost no effect on the phonon mode spectrum of a diamond crystal and the crystalline quality of the diamond lattice. This conclusion is reasonable under the assumption that fast electrons create no more than 30–40 ppm vacancies in the crystal lattice at the irradiation parameters used.

EPR spectroscopy of paramagnetic centers

Nitrogen and nickel impurities are present in the diamond lattice mainly in the neutral state (for N_S^0) and in the negatively charged state (for Ni_S^-). They have spins $S = 1/2$ and $S = 3/2$, respectively. In addition, a small amount of nitrogen is present in the system in charge state 1+ with spin $S = 0$ and in the form of non-paramagnetic dimers NN (so-called A-centers). Paramagnetic centers of nitrogen and nickel are easily detected by EPR. Figure 4, *a* shows the EPR spectrum for N_S^0 and Ni_S^- in powder sample #7381-*bis* at 100 K. The signal from paramagnetic nitrogen ($g = 2.0024$, the so-called P1 center [3]) has a pronounced triplet structure due to hyperfine splitting of the central signal induced by the magnetic moment of the nitrogen atom nucleus. The signal from Ni_S^- ($g = 2.0319$, the so-called W8 center [1,3,35]) is visible only at low temperatures, and at temperatures above 220 K it broadens so much as to become almost unobservable. Figure 4, *b* shows the EPR spectrum from centers N_S^0 (P1) and Ni_S^- (W8) after numerical integration. An integration procedure is used to correctly separate contributions from overlapping EPR signals and determine their basic characteristics, including integral intensity and full width at half height. The center line of the nitrogen triplet (P1) and the EPR signal from nickel (W8) are perfectly described by Lorentzian contours, which helps to separate the spectrum observed in the 316–331 mT magnetic field interval into their respective partial contributions and to estimate their integral intensities A_1 (for Ni_S^-) and A_2 (for N_S^0). The integral intensity of the central Lorentzian of signal P1 is, to a high degree of accuracy, 1/3 of integral intensity A_2 of the total P1 signal with account for both satellites of the hyperfine structure for the powder sample, and additional broad signals with the same g-factor ($g = 2.0024 \pm 0.0002$) under the central Lorentzian are virtually lacking or very insignificant in the EPR spectrum (Fig. 4, *b*). The latter indicates a lack or a negligible amount of cluster forms of paramagnetic nitrogen with spins 1/2, wherein all spins are coupled by magnetic exchange, in the material. In the case of diamond microcrystals synthesized by another method, this may not be the case, and cluster forms of paramagnetic nitrogen may be present [36].

Figure 5 shows the temperature characteristics of the main parameters of EPR signals from N_S^0 and Ni_S^- centers, such as linewidth, integral signal intensity, and/or ratio of integral signal intensities for both centers. The experimental points for the integral intensity of the N_S^0 signal are smoothed in the range of 100–200 K in accordance with the Curie–Weiss law by a hyperbolic function $\sim (T - \Theta)^{-1}$, where fitting parameter Θ (the so-called Weiss temperature) is $\Theta \sim -2$ K (Fig. 5, *a*). Almost the same inverse temperature proportionality is observed for the temperature variation of the signal from Ni_S^- centers. Thus, both centers are paramagnetic Curie-type centers with the integral intensity of the EPR signal being inversely proportional to temperature ($\sim T^{-1}$), but the dependences of signal widths on temperature differ for these centers (Fig. 5, *b*). The width of the central component of the EPR signal for N_S^0 is $\Delta H_{1/2} = 0.206$ mT at 200 K[4]. The corresponding width of the Lorentzian EPR signal in the spectrum of the first derivative (peak-to-peak distance) is $\Delta H_{pp} = \Delta H_{1/2}/1.7321 = 0.119$ mT. Applying the empirical

[3] Approximately $65 \cdot 10^3$ elementary emitters are present in this case in the focal waist of focused light with a length of $\sim 12.8\,\mu$m and a diameter of $2\,\mu$m (in the smallest cross-section).

[4] Here, $\Delta H_{1/2}$ is the width of the Lorentzian contour at half-height (for the spectrum obtained by numerical integration of the experimental spectrum of the first derivative of absorption with respect to magnetic field).

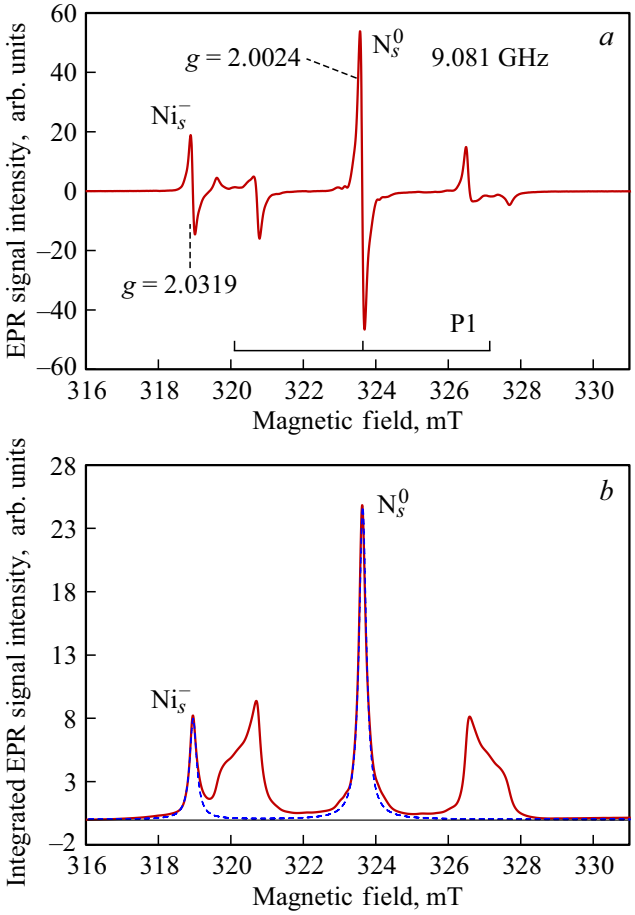

Figure 4. EPR spectrum of microcrystalline diamond powder #7381-*bis* in the $g \sim 2$ region at a temperature of 100 K: the recorded spectrum (*a*) and the same spectrum after numerical integration (*b*). Panel (*b*): dark red line — integral spectrum, dashed line — approximation of the central signal from N_S^0-centers and the low-field signal from Ni_S^-- centers by two Lorentzian contours. Microwave power — 1 μW, magnetic field modulation — 0.03 mT, and microwave frequency — 9.081 GHz. The magnetic induction values along the abscissa axis are not corrected.

van Wyck formula [5] relating the EPR line width of paramagnetic nitrogen to its concentration $[N_S^0]$ expressed in units of ppm, one may estimate the $[N_S^0]$ concentration at approximately 108 ppm [37]. For paramagnetic nitrogen, the width of the central component depends very weakly on temperature and has a slight tendency to broaden with decreasing T, whereas strong broadening is observed at temperatures above 130 K for the signal from Ni_S^- centers. The latter is related to the peculiarities of nickel spin 3/2, its partial delocalization within the nearest-neighbor carbon atoms and interaction with the phonon subsystem of the diamond lattice [22]. While spin-lattice relaxation accounts for the sharp broadening of the W8 signal from Ni_S^- centers at $T > 130$ K, the width of the W8 signal at $T < 120$ K is determined only by the dipole–dipole interaction of the nickel spin with the surrounding "gas" of paramagnetic centers of all types in the lattice [22]. In the temperature range of 100–110 K, the width of the W8 signal is $\Delta H_{1/2} = 0.232$ mT, while the width of the main line of triplet P1 from N_S^0 centers has almost the same value ($\Delta H_{1/2} = 0.238$ mT) in the same temperature range. This means that at $T < 120$ K, the signals from paramagnetic centers W8 and P1 are equally broadened under the influence of the predominant paramagnetic agents in the system: isolated nitrogen atoms. Despite the broadening of the EPR signal of Ni_S^- with increasing T, the dependence of its integral intensity on temperature at $T > 130$ K follows the Curie law ($\sim T^{-1}$) within the entire studied temperature range of 100–210 K, and the ratio of integral intensities of EPR signals from both centers $A_1/A_2 \sim 0.104$ is a constant within the accuracy of experimental data processing (Fig. 5, *c*). Hereinafter, indices 1 and 2 of various quantities correspond to nickel Ni_S^- and nitrogen N_S^0 centers, respectively.

Let us estimate the concentration of nickel centers in the system based on data on the ratio of signal intensities. Ratio A_1/A_2 of integral intensities of EPR signals from centers Ni_S^- and N_S^0 with different spins ($S_1 = 3/2$ and $S_2 = 1/2$) is related to the ratio of concentrations (N_1/N_2) of these spins in the material in the following way [38]:

$$\frac{A_1}{A_2} = \frac{N_1}{N_2}\frac{S_1(S_1+1)}{S_2(S_2+1)}\frac{g_1^2}{g_2^2} = 5\frac{N_1}{N_2}\frac{g_1^2}{g_2^2}.$$

Here, $N_{1,2}$ are the concentrations of spins of both types in the studied material and $g_{1,2}$ are the Lande factors for the corresponding paramagnetic centers with spins $S_1 = 3/2$ and $S_2 = 1/2$. For the two analyzed center types Ni_S^- (1) and N_S^0 (2), ratio

$$\frac{g_1^2}{g_2^2} = \frac{2.0319^2}{2.0024^2} \approx 1.0297,$$

and multiplier $\frac{S_1(S_1+1)}{S_2(S_2+1)} = 5$. Consequently, the concentration of nickel centers $[Ni_S^-]$ in the material can be calculated from the concentration of nitrogen centers defined above using the formula

$$N_1 = N_2\frac{A_1}{A_2}\frac{1}{5.148} = 108\,\text{ppm} \times 0.104 \times 0.194 \approx 2.2\,\text{ppm}.$$

Thus, the diamond matrix contains centers N_S^0 and Ni_S^- in amounts of ~ 108 ppm and ~ 2.2 ppm. This ratio is valid in the studied temperature range of 100–210 K. The presence of nickel centers with a concentration ~ 50 times lower than that of paramagnetic nitrogen should not affect in any significant way the photophysics of nitrogen centers and, consequently, fluorescent centers NV^-. Note that the obtained concentration of centers N_S^0 in the #7381-*bis* sample is slightly reduced compared to the corresponding value for non-irradiated #7381-un crystals.

[5] This formula is given in [37].

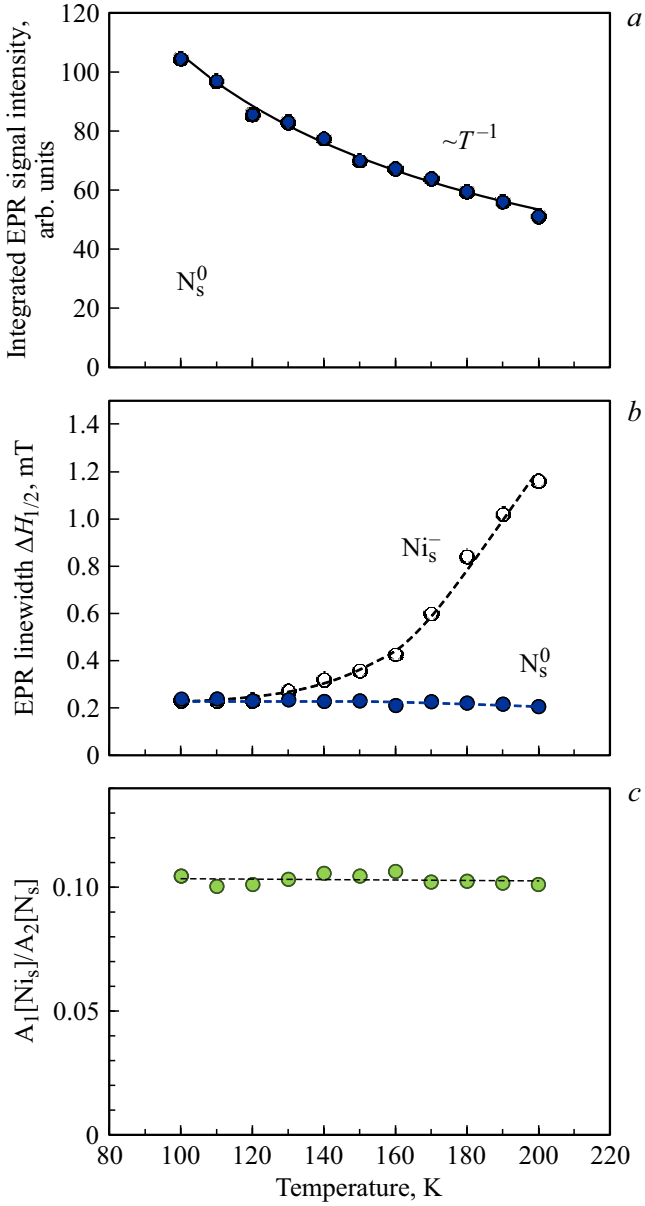

Figure 5. Temperature dependences of EPR signal parameters: (*a*) integral signal intensity for N_S^0, (*b*) $\Delta H_{1/2}$ linewidth for centers N_S^0 and Ni_S^-, and (*c*) ratio of integral signal intensities for centers Ni_S^- and N_S^0. Microwave power — 1 μW and frequency — 9.081 GHz.

When microcrystals are irradiated with broadband light from a xenon lamp passed through an HA30 filter with a bandwidth of 320–770 nm, the EPR spectra of N_S^0 and Ni_S^- centers change slightly so that the amplitude of the EPR signal from nickel in the negatively charged state decreases and that from nitrogen in the neutral state increases. The corresponding difference EPR spectrum obtained by subtracting the dark spectrum from the EPR spectrum under illumination is shown in Fig. 6. The change in amplitudes of EPR signals is associated with photoionization and dynamic recharging of a fraction of the

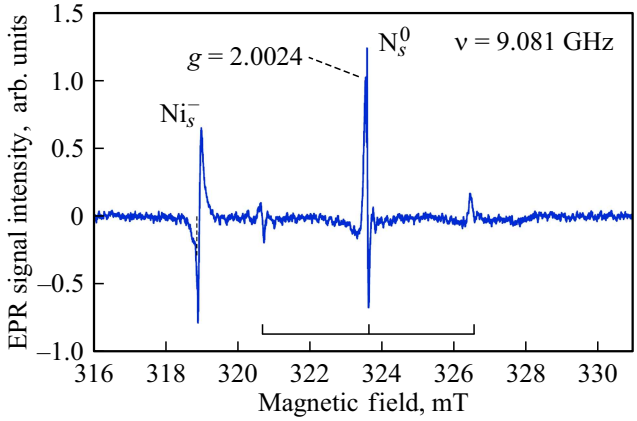

Figure 6. Difference EPR spectrum of microcrystalline diamond powder #7381-*bis* in the $g \sim 2$ range obtained by subtracting the dark spectrum from the spectrum recorded under illumination with light from a xenon lamp. The spectral range of excitation radiation is 320–770 nm. Microwave power — 1 μW, magnetic field modulation — 0.03 mT, and temperature $T = 100$ K. The magnetic induction values along the abscissa axis are not corrected.

centers and, as a consequence, the escape of electrons from some of the Ni_S^- centers to positively charged N_S^+ centers and other defects in the system. When Ni_S^- centers are photoionized, electrons first appear in the conduction band and are subsequently captured by the N_S^+ centers present in the system, which turn from non-paramagnetic to being paramagnetic with spin 1/2. The positions of energy levels of the corresponding centers are shown in the band diagram of diamond in Fig. 7.

EPR spectroscopy of the $\Delta m_s = 1$ and $\Delta m_s = 2$ transitions in NV^- centers

EPR spectra of microcrystalline powder #7381-*bis* in the range of 100–300 mT at temperatures of 100 and 293 K are shown in Fig. 8. The spectra are presented in their original form without subtraction of the background from superparamagnetic nickel nanoparticles possibly present in the lattice in small amounts. Signals in the region of 200–290 mT are associated with allowed x,y-transitions $\Delta m_s = 1$ and z-transitions $\Delta m_s = 1$ between Zeeman-split states of triplet level $^3A_2$ of the ground state of the NV^- center with magnetic quantum numbers $m_s = 0$ and $m_s = -1$. In this case, the signal from allowed z-transitions $\Delta m_s = 1$ is hard to see in the survey spectrum due to specific measurement conditions, but can be detected independently. In turn, the characteristic EPR signal in a half magnetic field at ~ 151 mT is associated with forbidden $\Delta m_s = 2$ transitions between the $m_s = -1$ and $m_s = 1$ states of the $^3A_2$ triplet level in a microwave field and has a g- factor $g = 4.295$[6] at frequency $\nu = 9.080$–9.081 GHz (Fig. 8). A diagram of

[6] According to the classifier of paramagnetic centers in diamond, EPR signals corresponding to NV^- centers are traditionally labelled as W15 [1,3].

$\Delta m_s = 2$ transitions is shown in Fig. 9. The calculated integral intensity of the $g = 4.295$ signal (W15) corresponds to a concentration of NV^- centers of about 4.5 ppm. A technique for estimating the concentration of NV^- centers with the use of reference synthetic diamond with a known NV^- concentration has been detailed earlier in [39].

The $g = 4.295$ (W15) signal associated with $\Delta m_s = 2$ transitions reveals a non-Curie character of the temperature dependence of the integral intensity and a weak dependence of width ΔH_{pp} [7] in the temperature range of 100–200 K. Thus, in contrast to the main EPR signal from N_S^0 centers and the signal from Ni_S^- centers, the integral intensity of the $g = 4.295$ (W15) signal practically does not change with decreasing temperature, and the width of this signal increases slightly with a decrease in T with a temperature coefficient of $-2.32 \cdot 10^{-4}$ mT/K. This fact is quite surprising, since the integral intensity of the $g = 4.295$ (W15) signal depends almost linearly on the square root of the microwave power in the 1–14 μW range (within the entire 100–293 K temperature range) and saturates only at high microwave powers in the resonator. The reason for this temperature behavior of the $g = 4.295$ (W15) signal requires separate consideration. Such an analysis should take into account the temperature dependence of the energy levels of the ground state $^3A_2$ ($m_s = 0, \pm 1$) of the triplet center, their splitting as a function of the lattice tension and their positioning relative to the Fermi level, and the temperature dependence of the spin-lattice relaxation time for the NV^- center. Illumination with xenon lamp radiation (using a combination of Hoya L42 and HA30 filters) at a temperature of 100 K leads to a several-fold amplification of the $g = 4.295$ (W15) signal due to optical spin polarization (Fig. 10), which induces a redistribution of populations of the ground state levels of the NV^- triplet center with magnetic quantum numbers $m_s = -1, 0, +1$ [40]. The signal is amplified by a fraction of diamond microcrystals in the quartz EPR tube that are adjacent to the inner walls of the tube in a layer of a certain thickness (of the order of several hundred micrometers) and absorb optical radiation in the range of 1.38–2.95 eV. With this illumination, the signal width (ΔH_{pp}) increases from 0.311 to 0.347 mT. The amplitude of the high-field component of the signal, which differs from the main component (at $g = 4.295$) by ~ 3 mT on the magnetic field scale (Fig. 10), is also amplified. Almost exactly the same $g = 4.295$ (W15) signal amplification occurs when xenon lamp radiation is transmitted through a single Hoya HA30 filter (with a spectral bandwidth of 1.38–4.1 eV). In turn, red and near-infrared light (1.38–1.94 eV) cut out from the spectrum of a xenon lamp by optical filters Hoya R64 and HA30 does not induce an increase in the amplitude of the $g = 4.295$ (W15) signal and, therefore, does not induce optical spin polarization for the $^3A_2$ ground state levels. Thus, the main contribution to optical spin polarization comes from the absorption of radiation in the 1.94–2.95 eV spectral band.

The determined characteristics correspond to synthetic microcrystalline Ib HPHT diamond with intense luminescence from NV^- centers. In this case, fluorescence radiation with a power of up to 2.5 μW and even more, depending on the geometry of focused radiation (when

[7] Here, we mean the ΔH_{pp} signal width in the spectrum of the first derivative of microwave absorption with respect to the magnetic field.

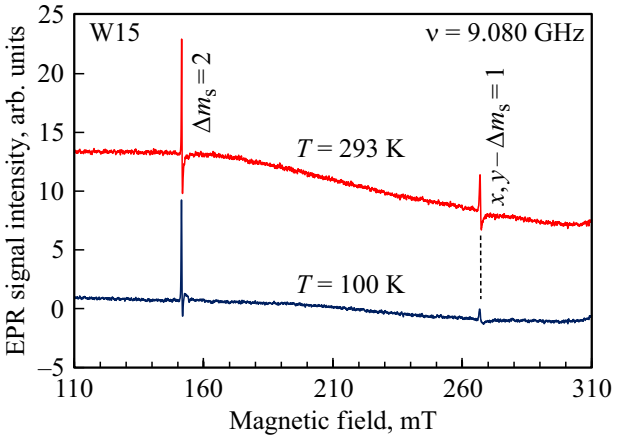

Figure 8. EPR spectra of microcrystalline diamond powder #7381-*bis* in the 110–310 mT range under dark conditions at temperatures of 100 (blue line) and 293 K (red line). Microwave power — 9.95 μW, magnetic field modulation — 0.1 mT, number of signal accumulations — 20, duration of a single spectrum pass — 120 s, and microwave frequency — 9.080 GHz. For ease of comparison, the spectra are shifted along the vertical axis.

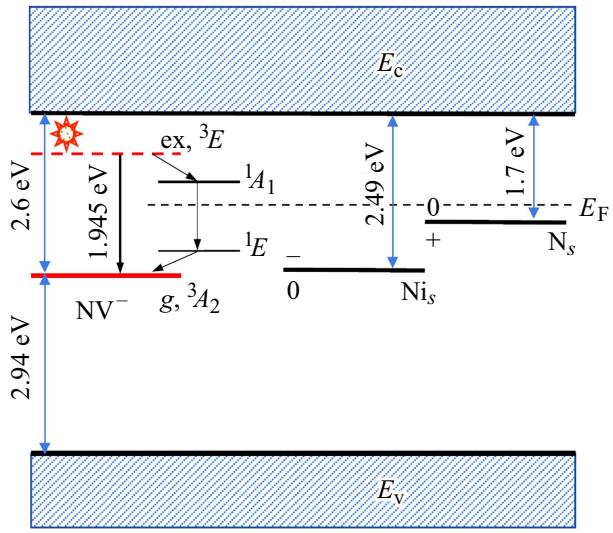

Figure 7. Band diagram of diamond with energy levels of centers NV^-, Ni_S, and N_S in the forbidden band. g, $^3A_2$, and ex, ^3E — ground and optically excited triplet states of the NV^- center, $^1A_1$ and ^1E — singlet states of the NV^- center inside the $^3A_2$–^3E gap responsible for the non-radiative recombination channel and optical emission at a wavelength of 1042 nm, E_F — Fermi level, and E_v and E_c — edges of the valence and conduction bands. The position of the Fermi level is schematic.

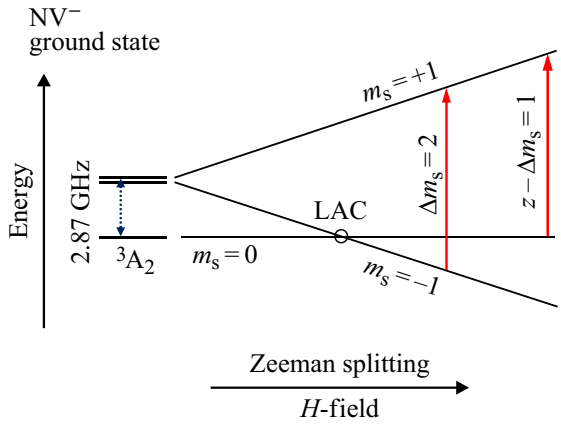

Figure 9. Diagram of forbidden ($\Delta m_s = 2$) and allowed (z-$\Delta m_s = 1$ microwave transitions in Zeeman-split levels of the ground triplet state of the NV^- center with its axis being collinear to magnetic field strength vector **H**. LAC is the anti-crossing point of the ground state levels of $^3A_2$ with magnetic quantum numbers 0 and −1 in a magnetic field of ∼ 100 mT.

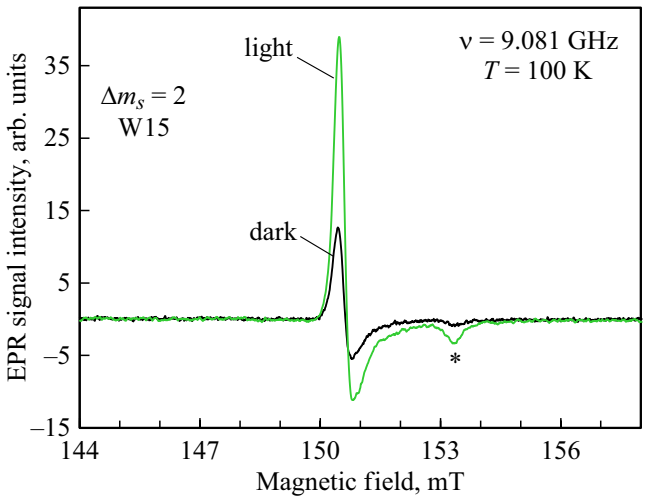

Figure 10. EPR spectra of microcrystalline diamond powder #7381-*bis* in the half magnetic field area recorded at 100 K under dark conditions (black line) and under illumination by the xenon lamp with a combination of Hoya L42 and HA30 filters (green line). Magnetic induction values along the abscissa axis are not corrected. A correction of +0.366 mT was used to calculate the g--factor of the EPR line.

excited by green laser light with an optical power of at least 15 mW) can be generated in the saturation mode in the focal waist area of excitation radiation focused onto a particle 13 μm in size. With optical feedback and additional surface treatment, the parameters of such microcrystals are quite sufficient to realize the laser effect in their volume [41,42]. The additional identification characteristics of microcrystals discovered in this work can be used to select fluorescent diamond microcrystals with the highest brightness and acceptable lattice quality. EPR spectroscopy provides estimates of the concentration of NV^- centers in microcrystals (∼ 4.5 ppm) consistent with the recorded NV^- luminescence intensity.

Conclusion

Microcrystals of synthetic Ib HPHT diamond with bright luminescence at NV^- centers contained in the crystal lattice at the ∼ 4.5 ppm level reveal a whole set of standard characteristics associated with lattice optical absorption, NV^- luminescence, and a Curie-type temperature dependence of EPR signals for impurities of paramagnetic nitrogen and nickel. At the same time, the temperature dependence of the EPR signal ($g = 4.295$) associated with „forbidden“ microwave transitions $\Delta m_s = 2$ between Zeeman-split levels of the ground state of the NV^- center and revealing the effect of optical spin polarization under irradiation with light with quanta energies of 1.94−2.95 eV does not follow the Curie's law, and the signal variies weakly in the 100−293 K range. This feature indicates a peculiar temperature dependence of levels of the ground triplet state of NV^- centers (with the effect of mechanical stress taken into account) and their special positioning relative to the Fermi level of the system and can be used to identify microcrystals with different required characteristics, including brightness ones.

Acknowledgment

V.Yu.O. would like to thank Columbus Nanoworks Ltd. (USA) and Professor Arfaan Rampersaud for providing the samples, as well as the Center for Micro- and Nanotechnology of Hosei University (Tokyo, Japan) for the opportunity to use diagnostic equipment and infrastructure of the Center.

Funding

This research was supported by the Russian Science Foundation (agreement 21-12-00264).

Information on the authors contribution

V.Yu. Osipov: problem statement, sample preparation, study of EPR signals at low temperatures, spectra processing and analysis, conceptualization, and preparation of the manuscript; F.M. Shakhov: infrared absorption study; K.V. Bogdanov: photoluminescence and Raman scattering studies; K. Takai: EPR spectrometer calibration and EPR spectroscopy data analysis; A.V. Baranov: optical data analysis and manuscript editing.

Conflict of interest

The authors declare that they have no conflict of interest within the scope of the study presented in this paper.

References

[1] A.M. Zaitsev. *Optical properties of diamond: A data handbook* (Springer–Verlag, Berlin–Heidelberg–NY., 2001). DOI: 10.1007/978-3-662-04548-0

[2] H.C. Chang, W.W.W. Hsiao, M.C. Su. *Fluorescent nanodiamonds* (John Wiley & Sons, Hoboken–Chichester–Oxford, 2019). DOI: 10.1002/9781119477099

[3] J.H.N. Loubser, J.A. van Wyck. Rep. Prog. Phys., **41**, 1201 (1978). DOI: 10.1088/0034-4885/41/8/002

[4] R.I. Mashkovtsev, Yu.N. Pal'yanov. Sol. St. Commun., **111**, 397 (1999). DOI: 10.1016/S0038-1098(99)00180-5

[5] A.I. Shames, A. Dalis, A.D. Greentree, B.C. Gibson, H. Abe, T. Ohshima, O. Shenderova, A. Zaitsev, P. Reineck. Adv. Opt. Mater., **8**, 2001047 (2020). DOI: 10.1002/adom.202001047

[6] O.A. Shenderova, A.I. Shames, N.A. Nunn, M.D. Torelli, I. Vlasov, A. Zaitsev. J. Vac. Sci. Technol. B, 37 (3), 030802 (2019). DOI: 10.1116/1.5089898

[7] M.W. Doherty, N.B. Manson, P. Delaney, F. Jelezko, J. Wrachtrup, L.C. L. Hollenberg. Phys. Rep., **528** (1), 1 (2013). DOI: 10.1016/j.physrep.2013.02.001

[8] J.P. Boudou, P.A. Curmi, F. Jelezko, J. Wrachtrup, P. Aubert, M. Sennour, G. Balasubramanian, R. Reuter, A. Thorel, E. Gaffet. Nanotechnology, **20**, 235602 (2009). DOI: 10.1088/0957-4484/20/23/235602

[9] A.I. Shames, V.Y. Osipov, J.P. Boudou, A.M. Panich, H.J. von Bardeleben, F. Treussart, A.Y. Vul'. J. Phys. D, **48** (15), 155302 (2015). DOI: 10.1088/0022-3727/48/15/155302

[10] K. Jensen, P. Kehayias, D. Budker. Smart Sensors, Measurement and Instrumentation **19**, 553 (2017). DOI: 10.1007/978-3-319-34070-8_18

[11] V.M. Acosta, E. Bauch, M.P. Ledbetter, C. Santori, K.-M.C. Fu, P.E. Barclay, R.G. Beausoleil, H. Linget, J.F. Roch, F. Treussart, S. Chemerisov, W. Gawlik, D. Budker. Phys. Rev. B, **80**, 115202 (2009). DOI: 10.1103/physrevb.80.115202

[12] M. Fujiwara, Y. Shikano. Nanotechnology, **32**, 482002 (2021). DOI: 10.1088/1361-6528/ac1fb1

[13] G. Kucsko, P.C. Maurer, N.Y. Yao, M. Kubo, H.J. Noh, P.K. Lo, H. Park, M.D. Lukin. Nature, **500** (7460), 54 (2013). DOI: 10.1038/nature12373

[14] K.O. Ho, M.Y. Leung, Y. Jiang, K.P. Ao, W. Zhang, K.Y. Yip, Y.Y. Pang, K.C. Wong, S.K. Goh, S. Yang. Phys. Rev. Appl., **13**, 024041 (2020). DOI: 10.1103/PhysRevApplied.13.024041

[15] S. Hsieh, P. Bhattacharyya, C. Zu, T. Mittiga, T.J. Smart, F. Machado, B. Kobrin, T.O. Hohn, N.Z. Rui, M. Kamrani, S. Chatterjee, S. Choi, M. Zaletel, V.V. Struzhkin, J.E. Moore, V.I. Levitas, R. Jeanloz, N.Y. Yao. Science, **366**, 1349 (2019). DOI: 10.1126/science.aaw4352

[16] S. Johnson, P.R. Dolan, J.M. Smith. Progr. Quant. Electron., **55**, 129 (2017). DOI: 10.1016/j.pquantelec.2017.05.003

[17] M.J. Degen. *On the creation, coherence and entanglement of multi-defect quantum registers in diamond* (Ph. D. thesis, Delft University of Technology, Delft, 2021). DOI: 10.4233/uuid:e0b20592-a0ce-4ec4-8df0-a5aa25084301

[18] O. Faklaris, V. Joshi, T. Irinopoulou, P. Tauc, M. Sennour, H. Girard, C. Gesset, M. Senour, A. Thorel, J.-C. Arnault, J.-P. Boudou, P.A. Curmi, F. Treussart. ACS Nano, **3**, 3955 (2009). DOI: 10.1021/nn901014j

[19] D. Duan, G.X. Du, V.K. Kavatamane, S. Arumugam, Y.K. Tzeng, H.C. Chang, G. Balasubramanian. Optics Express, **27**, 6734 (2019). DOI: 10.1364/OE.27.006734

[20] W.V. Smith, P.P. Sorokin, I.L. Gelles, G.J. Lasher. Phys. Rev., **115**, 1546 (1959). DOI: 10.1103/PhysRev.115.1546

[21] J.H.N. Loubser, W.P. van Ryneveld. Nature, **211**, 517 (1966). DOI: 10.1038/211517a0

[22] J. Isoya, H. Kanda, J.R. Norris, J. Tang, M.K. Bowman. Phys. Rev. B, **41**, 3905 (1990). DOI: 10.1103/physrevb.41.3905

[23] A.I. Shames, V.Y. Osipov, K.V. Bogdanov, A.V. Baranov, M.V. Zhukovskaya, A. Dalis, S.S. Vagarali, A.J. Rampersaud. J. Phys. Chem. C, **121** (9), 5232 (2017). DOI: 10.1021/acs.jpcc.6b12827

[24] K.V. Bogdanov, M.V. Zhukovskaya, V.Yu. Osipov, E.V. Ushakova, M.A. Baranov, K. Takai, A. Rampersaud, A.V. Baranov. APL Materials, **6** (8), 086104 (2018). DOI: 10.1063/1.5045535

[25] V.Yu. Osipov, N.M. Romanov, K.V. Bogdanov, F. Treussart, C. Jentgens, A. Rampersaud. J. Opt. Technol., **85** (2), 63 (2018). DOI: 10.1364/JOT.85.000063

[26] M.N.R. Ashfold, J.P. Goss, B.L. Green, P.W. May, M.E. Newton, C.V. Peaker. Chem. Rev., **120**, 5745 (2020). DOI: 10.1021/acs.chemrev.9b00518

[27] G.S. Woods, J.A. van Wyck, A.T. Collins. Phil. Mag. B, **62**, 589 (1990). DOI: 10.1080/13642819008215257

[28] G. Davies. Physica B, **273/274**, 15 (1999). DOI: 10.1016/s0921-4526(99)00398-1

[29] S.C. Lawson, D. Fisher, D.C. Hunt, M.J. Newton. J. Phys.: Cond. Matt., **10**, 6171 (1998). DOI: 10.1088/0953-8984/10/27/016

[30] L.J. Su, C.Y. Fang, Y.T. Chang, K.M. Chen, Y.C. Yu, J.H. Hsu, H.C. Chang. Nanotechnology, **24**, 315702 (2013). DOI: 10.1088/0957-4484/24/31/315702

[31] *Optical Engineering of Diamond*, 1st Edition, ed. by R.P. Mildren and J.R. Rabeau (Wiley-VCH Verlag GmbH & Co. KGaA, Weinheim, 2013). ISBN: 978-3-527-64862-7

[32] Z.Z. Liang, X. Jia, H.A. Ma, C.Y. Zang, P.W. Zhu, Q.F. Guan, H. Kanda. Diam. Relat. Mater., **14**, 1932 (2005). DOI: 10.1016/j.diamond.2005.06.041

[33] G. Davies. In: *Chemistry and Physics of Carbon: A Series of Advances*, ed. by P.L. Walker Jr., P.A. Thrower. Book series (Marcel Dekker, Inc., NY., 1977), vol. 13, pp. 1-143. https://cir.nii.ac.jp/crid/1573387451279760128

[34] F.M. Shakhov, V.Yu. Osipov, A.A. Krasilin, K. Iizuka, R. Oshima. J. Sol. St. Chem., **307**, 122804 (2022). DOI: 10.1016/j.jssc.2021.122804

[35] A.T. Collins, H. Kanda, J. Isoya, C.A.J. Ammerlaan, J.A. van Wyk. Diam. Relat. Mater., **7** (2-5), 333 (1998). DOI: 10.1016/s0925-9635(97)00270-7

[36] V.Yu. Osipov, F.M. Shakhov, N.N. Efimov, V.V. Minin, S.V. Kidalov, A.Ya. Vul'. Phys. Solid State, **59**, 1146 (2017). DOI: 10.1134/S1063783417060191

[37] J.A. van Wyck, E.C. Reynhardt, G.L. High, I. Kiflawi. J. Phys. D, **30**, 1790 (1997). DOI: 10.1088/0022-3727/30/12/016

[38] V.Yu. Osipov, F.M. Shakhov, N.M. Romanov, K. Takai. Mendeleev Commun., **32**, 645 (2022). DOI: 10.1016/j.mencom.2022.09.026

[39] V.Yu. Osipov, F. Treussart, S.A. Zargaleh, K. Takai, F.M. Shakhov, B.T. Hogan, A. Baldycheva. Nanoscale Res. Lett., **14** (1), 279 (2019). DOI: 10.1186/s11671-019-3111-y

[40] V.Yu. Osipov, K.V. Bogdanov, A. Rampersaud, K. Takai, Y. Ishiguro, A.V. Baranov. Opt. Spektrosk., **130**, 1922 (2022). DOI: 10.21883/OS.2022.12.54101.4248-22

[41] J. Jeske, D.W.M. Lau, X. Vidal, L.P. McGuinness, P. Reineck, B.C. Johnson, M.W. Doherty, J.C. McCallum, S. Onoda, F. Jelezko, T. Oshima, T. Volz, J.H. Cole, B.C. Gibson, A.D. Greentree. Nat. Commun., **8**, 14000 (2017). DOI: 10.1038/ncomms14000
[42] A. Savvin, A. Dormidonov, E. Smetanina, V. Mitrokhin, E. Lipatov, D. Genin, S. Potanin, A. Yelisseyev, V. Vins. Nat. Commun., **12**, 7118 (2021). DOI: 10.1038/s41467-021-27470-7

Translated by D.Safin